Sub-milliampere threshold operation of butt-jointed built-in membrane DFB laser bonded on Si substrate

Daisuke Inoue,[1,*] Jieun Lee,[1] Takuo Hiratani,[1] Yuki Atsuji,[1] Tomohiro Amemiya,[2] Nobuhiko Nishiyama,[1] and Shigehisa Arai[1,2]

[1]*Department of Electrical and Electronic Engineering, Tokyo Institute of Technology,2-12-1-S9-5 O-okayama, Meguro-ku, Tokyo 152-8552, Japan*

[2]*Quantum Nanoelectronics Research Center, Tokyo Institute of Technology, 2-12-1-S9-5 O-okayama, Meguro-ku, Tokyo 152-8552, Japan*

[*]*inoue.d.ac@m.titech.ac.jp*

Abstract: We fabricated GaInAsP/InP waveguide-integrated lateral-current-injection (LCI) membrane distributed feedback (DFB) lasers on a Si substrate by using benzocyclobutene (BCB) adhesive bonding for on-chip optical interconnection. The integration ofa butt-jointed built-in (BJB) GaInAsP passive waveguide was performed by organometallic vapor-phase epitaxy (OMVPE).By introducing a strongly index-coupled DFB structure with a 50-μm-long cavity, a threshold current of 230 μA was achieved for a stripe width of 0.8 μm under room-temperature continuous-wave (RT-CW) conditions. The maximum output power of 32 μW was obtained. The lasing wavelength and submode suppression ratio (SMSR) were 1534 nm and 28 dB, respectively, at a bias current of 1.2 mA.

OCIS codes: (230.0230) Optical devices; (140.3490) Lasers, distributed-feedback; (200.4650) Optical interconnects; (250.5960) Semiconductor lasers.

References and links

1. G. E. Moore, "Cramming more components onto integrated circuits," Electronics **38**, 114–117 (1965).
2. P. Kapur, J. P. McVittie, and K. C. Saraswat, "Technology and reliability constrained future copper interconnects. I. Resistance modeling," IEEE Trans. Electron. Dev. **49**(4), 590–597 (2002).
3. P. Kapur, G. Chandra, J. P. McVittie, and K. C. Saraswat, "Technology and reliability constrained future copper interconnects. II. Performance implications," IEEE Trans. Electron. Dev. **49**(4), 598–604 (2002).
4. D. A. B. Miller, "Device requirements foroptical interconnects to silicon chips," Proc. IEEE **97**(7), 1166–1185 (2009).
5. W. Hofmann, M. Müller, A. Nadtochiy, C. Meltzer, A. Mutig, G. Böhm, J. Rosskopf, D. Bimberg, M. C. Amann, and C. Chang-Hasnain, "22-Gb/s long wavelength VCSELs," Opt. Express **17**(20), 17547–17554 (2009).
6. S. Imai, K. Takaki, S. Kamiya, H. Shimizu, J. Yoshida, Y. Kawakita, T. Takagi, K. Hiraiwa, H. Shimizu, T. Suzuki, N. Iwai, T. Ishikawa, N. Tsukiji, and A. Kasukawa, "Recorded low power dissipation in highly reliable 1060-nm VCSELs for 'Green' optical interconnection," IEEE J. Sel. Top. Quantum Electron. **17**(6), 1614–1620 (2011).
7. P. Moser, J. A. Lott, and D. Bimberg, "Energy efficiency of directly modulated oxide-confined high bit rate 850-nm VCSELs for optical interconnects," IEEE J. Sel. Top. Quantum Electron. **19**(4), 1702212 (2013).
8. S. Matsuo, A. Shinya, C.-H. Chen, K. Nozaki, T. Sato, Y. Kawaguchi, H. Taniyama, and M. Notomi, "20-Gbit/s directly modulated photonic crystal nanocavity laser with ultra-low power consumption," Opt. Express **19**(3), 2242–2250 (2011).
9. S. Matsuo, K. Takeda, T. Sato, M. Notomi, A. Shinya, K. Nozaki, H. Taniyama, K. Hasebe, and T. Kakitsuka, "Room-temperature continuous-wave operation of lateral current injection wavelength-scale embedded active-region photonic-crystal laser," Opt. Express **20**(4), 3773–3780 (2012).
10. K. Takeda, T. Sato, A. Shinya, K. Nozaki, W. Kobayashi, H. Taniyama, M. Notomi, K. Hasebe, T. Kakitsuka, and S. Matsuo, "Few-fJ/bit data transmissions using directly modulated lambda-scale embedded active region photonic-crystal lasers," Nat. Photonics **7**(7), 569–575 (2013).

#232433 - $15.00 USD Received 13 Jan 2015; revised 6 Mar 2015; accepted 9 Mar 2015; published 17 Mar 2015

11. T. Mikawa, M. Kinoshita, K. Hiruma, T. Ishitsuka, M. Okabe, S. Hiramatsu, and M. Bonkohara, "Implementation of active interposer for high-speed and low-cost chip level optical interconnects," IEEE J. Sel. Top. Quantum Electron. **9**(2), 452–459 (2003).
12. C.-T. Chen, P.-K. Shen, T.-Z. Zhu, C.-C. Chang, S.-S. Lin, M.-Y. Zeng, C.-Y. Chiu, H.-L. Hsiao, H.-C. Lan, Y.-C. Lee, Y.-C. Lin, and M.-L. Wu, "Chip-level 1 × 2 opticalinterconnects using polymer vertical splitter on silicon substrate," IEEE Photon. J. **6**(2), 7900410 (2014).
13. S. Arai, N. Nishiyama, T. Maruyama, and T. Okumura, "GaInAsP/InP membrane lasers for optical interconnects," IEEE J. Sel. Top. Quantum Electron. **17**(5), 1381–1389 (2011).
14. T. Shindo, M. Futami, T. Amemiya, N. Nishiyama, and S. Arai, "Design of Lateral-Current-Injection-Type Membrane Distributed-Feedback Lasers for On-Chip Optical Interconnections," IEEE J. Sel. Top. Quantum Electron. **19**(4), 1502009 (2013).
15. T. Okamoto, N. Nunoya, Y. Onodera, S. Tamura, and S. Arai, "Continuous wave operation of optically pumped membrane DFB laser," Electron. Lett. **37**(24), 1455–1457 (2001).
16. T. Okamoto, N. Nunoya, Y. Onodera, T. Yamazaki, S. Tamura, and S. Arai, "Optically pumped membrane BH-DFB lasers for low-threshold and single-mode operation," IEEE J. Sel. Top. Quantum Electron. **9**(5), 1361–1366 (2003).
17. S. Sakamoto, H. Naitoh, M. Ohtake, Y. Nishimoto, T. Maruyama, N. Nishiyama, and S. Arai, "85 °C continuous-wave operation of GaInAsP/InP-membrane buried heterostructure distributed feedback lasers with polymer cladding layer," Jpn. J. Appl. Phys. **46**(47), L1155–L1157 (2007).
18. K. Oe, Y. Noguchi, and C. Caneau, "GaInAsP lateral current injection lasers on semi-insulating substrates," IEEE Photon. Technol. Lett. **6**(4), 479–481 (1994).
19. T. Okumura, M. Kurokawa, M. Shirao, D. Kondo, H. Ito, N. Nishiyama, T. Maruyama, and S. Arai, "Lateral current injection GaInAsP/InP laser on semi-insulating substrate for membrane-based photonic circuits," Opt. Express **17**(15), 12564–12570 (2009).
20. T. Okumura, H. Ito, D. Kondo, N. Nishiyama, and S. Arai, "Continuous wave operation of thin film lateral current injection lasers grown on semi-insulating InP substrate," Jpn. J. Appl. Phys. **49**(4 4R), 040205 (2010).
21. T. Shindo, T. Okumura, H. Ito, T. Koguchi, D. Takahashi, Y. Atsumi, J. Kang, R. Osabe, T. Amemiya, N. Nishiyama, and S. Arai, "GaInAsP/InP lateral-current-injection distributed feedback laser with a-Si surface grating," Opt. Express **19**(3), 1884–1891 (2011).
22. D. Inoue, J. Lee, K. Doi, T. Hiratani, Y. Atsuji, T. Amemiya, N. Nishiyama, and S. Arai, "Room-temperature continuous-wave operation of GaInAsP/InP lateral-current-injection membrane laser bonded on Si substrate," Appl. Phys. Express **7**(7), 072701 (2014).
23. Y. Abe, K. Kishino, Y. Suematsu, and S. Arai, "GaInAsP/InP integrated laser with butt-jointed built-in distributed-Bragg-reflection waveguide," Electron. Lett. **17**(25), 945–947 (1981).
24. D. Inoue, J. Lee, T. Shindo, M. Futami, K. Doi, T. Amemiya, N. Nishiyama, and S. Arai, "Butt-joint built-in (BJB) structure for membrane photonic integration," The 25th International Conference on Indium Phosphide and RelatedMaterials (IPRM 2013), Kobe, Japan, TuD3–6,May (2013).
25. K. Kudo, J. Shim, K. Komori, and S. Arai, "Reduction of effective linewidth enhancement factor α_{eff} of DFB lasers with complex coupling coefficients," IEEE Photon. Technol. Lett. **4**(6), 531–534 (1992).
26. K. Ohira, T. Murayama, S. Tamura, and S. Arai, "Low-threshold and high-efficiency operation of distributed reflector lasers with width-modulated wirelike active regions," IEEE J. Sel. Top. Quantum Electron. **11**(5), 1162–1168 (2005).
27. T. Hiratani, K. Doi, Y. Atsuji, T. Amemiya, N. Nishiyama, and S. Arai, "Low-power and high-speed operation capabillities of semiconductor membrane lasers – energy cost limited by joule heat," The 26th International Conference on Indium Phosphide and Related Materials (IPRM 2014), Montpellier, France, P29, May (2014).
28. J. Lee, Y. Maeda, Y. Atsumi, Y. Takino, N. Nishiyama, and S. Arai, "Low-loss GaInAsP wire waveguide on Si substrate with benzocyclobutene adhesive wafer bonding for membrane photonic circuits," Jpn. J. Appl. Phys. **51**(4), 042201 (2012).

1. Introduction

The progress of state-of-the-art microprocessor has been promoted by the scaling law along with Moore's law [1]. However, there are serious problems associated with the global copper electrical wiring, such as heating bottlenecks and RC delays [2,3]. If further scaling reductions are carried out, the global copper wiring will restrict the performance of large-scale-integrated circuit (LSI) chips. As a substitute for the electrical global wiring, an on-chip optical interconnection has been extensively investigated. In order to create densely integrated on-chip optical circuits, a small and ultralow-energy-consumption light source is an essential component. In such an application, the available energy cost of the transmitter is estimated to be significantly less than 100 fJ/bit [4]. Several ultralow-power-consumption semiconductor lasers have already been reported, e.g., vertical-cavity surface-emitting lasers (VCSELs) [5–7] or photonic-crystal (PhC) lasers [8–10]. VCSELs have been widely used in short-reach

#232433 - $15.00 USD Received 13 Jan 2015; revised 6 Mar 2015; accepted 9 Mar 2015; published 17 Mar 2015

communications because of their low power consumption and high efficiency characteristics. However, in terms of the on-chip application of VCSELs, the disadvantage is that their light output is emitted perpendicular to the substrate. Therefore, the integration of a micromirror is needed for on-chip application [11,12].Electrically driven PhC lasers have operated with an energy cost of 4.4fJ/bit under room-temperature continuous-wave (RT-CW) conditions [10]. However, an avalanche photodiode, which requires a high applied voltage and has a relatively high energy consumption, was used in this measurement because the output power from the laser was not sufficient for PIN photodiodes. Thus, there have been no reports on lasers with ultralow power consumption, in-plane integration, and sufficient output power.

For the realization of a light source that satisfies these requirements, we have proposed and experimentally demonstrate dIII–V semiconductor membrane distributed feedback (DFB) lasers for the light source of an on-chip optical interconnection [13].The membrane structure consists of a thin semiconductor core layer sandwiched between dielectric cladding layers with low-refractive-index materials such as air, SiO_2,and benzocyclobutene (BCB). The large refractive-index difference produced by this structure leads to strong optical confinement in the core layer and strong index-coupling of the DFB grating. Therefore, the membrane DFB lasers can achieve ultralow threshold operation with an extremely short cavity structure [14]. In order to prepare the membrane structure, the BCB adhesive bonding technique offers good results with CMOS-process-compatible temperatures. Previously, we reported RT-CW operation of a membrane DFB laser under optical pumping [15], its low-threshold operation [16], and CW operation up to 85°C [17].For the electrically pumped operation of a membrane laser, we introduced a lateral-current-injection (LCI) structure [18] and reported top air-clad LCI Fabry–Perot (FP) lasers prepared on a semi-insulating InP substrate [19,20] and DFB lasers with an amorphous Si surface grating [21].Recently, we have demonstrated RT-CW operation of a membrane FP laser on a Si substrate [22]. However, the introduction of a strongly index-coupled DFB structure with a short cavity length is necessary to achieve low-threshold-current operation of a membrane DFB laser.

In this paper, we report waveguide-integrated LCI-membrane DFB lasers bonded on a Si substrate. By introducing a butt-jointed built-in (BJB) integrated structure [23], we could easily form short-cavity DFB lasers with a strongly index-coupled surface grating structureformed on an InP cap layer. As a result, we could demonstrate RT-CW operation of the BJB membrane DFB laser with a very low threshold current of 230 μA for a cavity length of 50 μm and a stripe width of 0.8μm.

2. Device structure and fabrication

Figure 1 shows a schematic of the initial wafer structure that consists of GaInAs (undoped, 300 nm thick) and InP (undoped, 100 nm thick) etch-stop layers, a p^+-GaInAs contact layer ($N_A = 8 \times 10^{18}$ cm^{-3}, 50 nm), a p-InP cap layer ($N_A = 1 \times 10^{18}$ cm^{-3}, 100 nm), five 1% compressively strained $Ga_{0.22}In_{0.78}As_{0.81}P_{0.19}$quantum wells (undoped, 6 nm)with 0.15% tensile strained $Ga_{0.26}In_{0.74}As_{0.49}P_{0.51}$ barriers (undoped, 10 nm) sandwiched by $Ga_{0.21}In_{0.79}As_{0.46}P_{0.54}$optical confinement layers (OCLs; undoped, 15 nm), and an InP cap layer (undoped, 50 nm). These layers were grown on a (100) n-InP substrate by gas-source molecular-beam epitaxy (MBE).

#232433 - $15.00 USD Received 13 Jan 2015; revised 6 Mar 2015; accepted 9 Mar 2015; published 17 Mar 2015

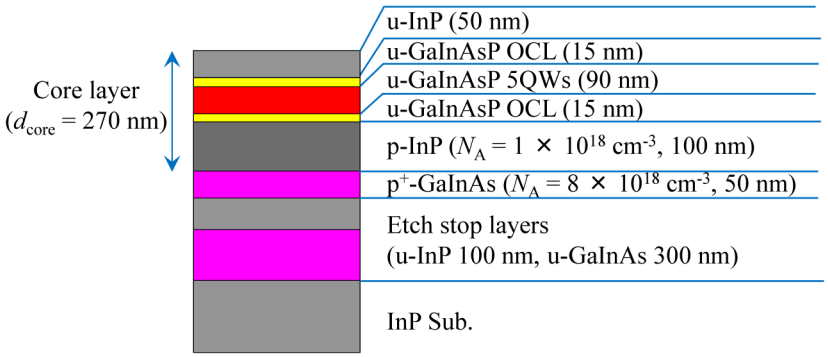

Fig. 1. Initial wafer structure.

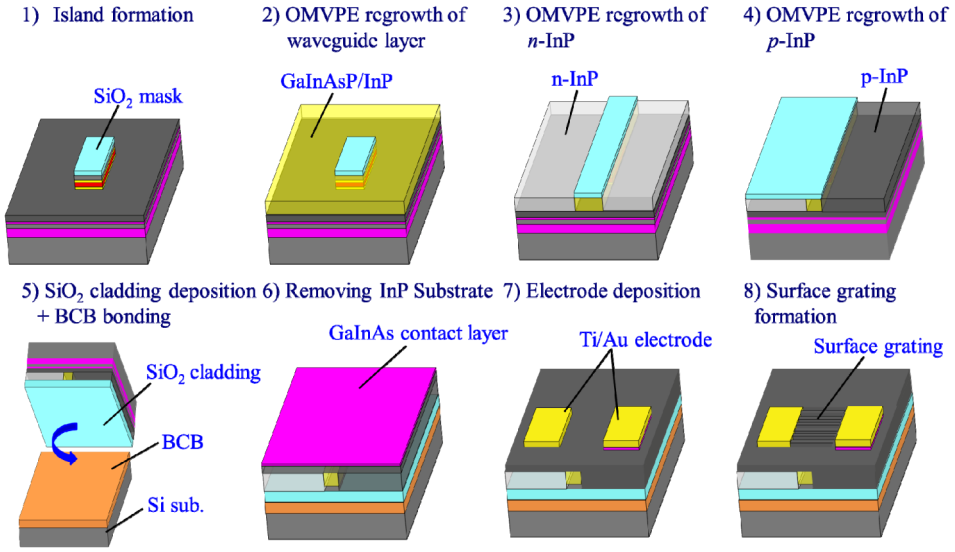

Fig. 2. Fabrication process of a waveguide-integrated LCI-membrane DFB laser.

Figure 2 shows the fabrication process of the waveguide-integrated LCI-membrane DFB laser. First, an island-shaped mesa structure of the active region was formed along the [011] direction by CH_4/H_2 reactive-ion etching (RIE) and selective wet chemical etching with a 50-nm-thick SiO_2 mask. The island width was 10 µm, and the length was varied between 20 and 300 µm. Then, regrowth of the GaInAsP waveguide layer for the BJB structure was carried out by organometallic vapor-phase epitaxy (OMVPE). In this regrowth process, a 10-nm-thick InP layer was first grown at 600°C; then, a 150-nm-thick $Ga_{0.21}In_{0.79}As_{0.46}P_{0.54}$layer and 20-nm-thick InP cap layer were grown at 650°C. Next, a 7-µm-wide mesa structure was formed by using the same etching method as described above, and an n-InP layer ($N_D = 4 \times 10^{18}$ cm^{-3}) was regrown by OMVPE. Next, one side of the n-InP layer beside the stripe was etched, and a p-InP layer ($N_A = 4 \times 10^{18}$ cm^{-3})was regrown to form an LCI buried heterostructure with a stripe width of 1–2 µm. After the three-step regrowth process, a 1-µm-thick SiO_2 cladding layer was deposited onto the wafer by plasma-enhanced chemical-vapor deposition (PECVD). Then, the wafer was bonded upside-down onto a Si substrate with an intermediate BCB adhesive layer with a thickness of 2µm. The BCB layer was prepared by spincoating, followed by curing at 210°C in a N_2 atmosphere. Then, the wafer was bonded to the Si substrate at a pressure of 25 kPa at 130°C. After that, the bonded wafers were baked at 250°C for 1 h in aN_2 atmosphere for hard curing of the BCB adhesive layer. The upper InP substrate

#232433 - $15.00 USD Received 13 Jan 2015; revised 6 Mar 2015; accepted 9 Mar 2015; published 17 Mar 2015

side and etch-stop layers were removed by chemical polishing and selective wet chemical etching, thereby revealing the GaInAs contact layer. After this etching process, the total thickness of the membrane core layers became 270-nm.This contact layer was etched by selective wet etching, except for the p-side electrode region, and the p-InP cap layer on the n-side electrode region was removed to reveal the regrown n-InP layer. Ti/Au electrodes were deposited for both n- and p- type contacts. Finally, a surface grating structure was formed on the InP cap layer by wet chemical etching with a SiO_2 mask pattern defined by electron-beam lithography. Then, the processed wafer was cleaved into bar form at the waveguide section to measure the light-output characteristics. The facets had no antireflection coating because the membrane DFB lasers are light source for on-chip optical interconnection. Therefore the facet coating technique is not suitable approach. The residual reflectivity at the facet is estimated to be approximately 20%.

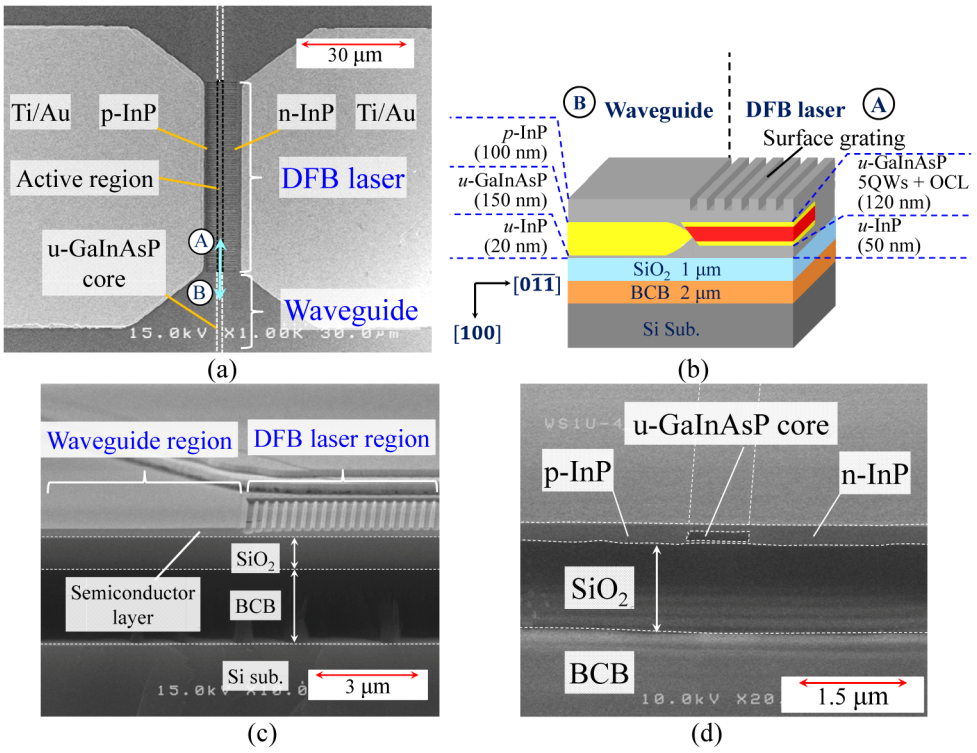

Fig. 3. (a) SEM image of the top view of the fabricated waveguide-integrated LCI-membrane DFB laser. (b) Schematic diagram of the cross section parallel to the stripe at the coupling section. (c) SEM image of the cross section parallel to the stripe observed at the coupling section. (d) SEM image of the cross section perpendicular to the stripe observed at the passive waveguide section.

#232433 - $15.00 USD Received 13 Jan 2015; revised 6 Mar 2015; accepted 9 Mar 2015; published 17 Mar 2015

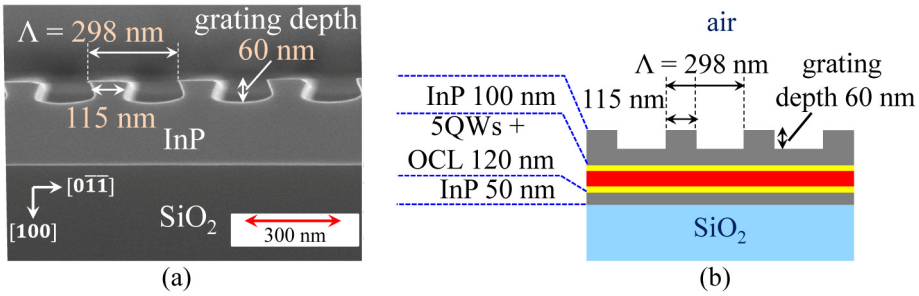

Fig. 4. (a) SEM image of the surface grating observed at the InP side cladding region beside the active-region stripe. (b) Calculated surface-grating structure approximated by a square shape.

Figure 3(a) shows an SEM image of the top view of the fabricated waveguide-integrated LCI-membrane DFB laser. Figures 3(b) and 3(c) show a schematic diagram of the cross section parallel to the stripe at the coupling section and its SEM image, respectively. Figure 3(d) shows an SEM image of the cross section perpendicular to the stripe observed at the passive waveguide section. Although the fabrication process includes a three-step regrowth process, we could successfully obtain an LCI buried heterostructure with a flat surface. The reflectivity due to BJB structure between the active and the passive region was calculated to be under –40dB by using finite difference and eigenmode expansion method [24].

Figure 4(a) shows an SEM image of the surface grating structure observed at the InP side cladding region beside the active-region stripe of the device. The surface grating was a trapezoidal shape with a depth of 60 nm and a mesa width of approximately 115 nm within the period of 298 nm. For simplicity, we estimated the index-coupling coefficient κ_i [25] by assuming that the grating shape is a square, as seen in Fig. 4(b). κ_i was calculated to be 1800 cm^{-1} for a depth of 60 nm and can be applied to realize a very short-cavity DFB laser with a strongly index-coupled grating structure.

3. Device characteristics

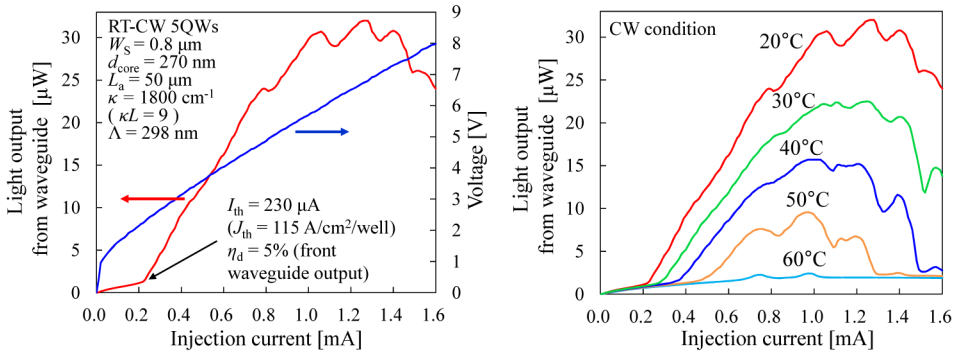

Fig. 5. (a) Light-output and voltage–current characteristics of a waveguide-integrated LCI-membrane DFB laser. (b) Light-output characteristics for various operating temperatures under CW condition.

#232433 - $15.00 USD Received 13 Jan 2015; revised 6 Mar 2015; accepted 9 Mar 2015; published 17 Mar 2015

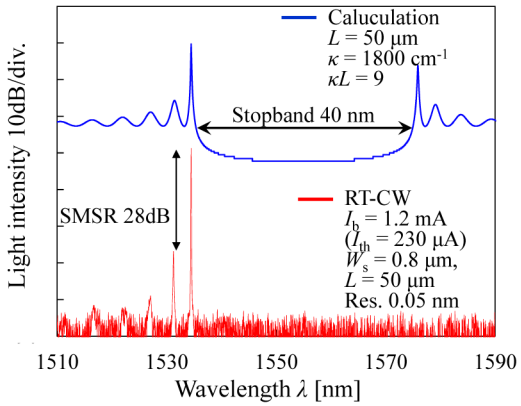

Fig. 6. Lasing spectrum for a device with a cavity length of 50 μm and a stripe width of 0.8 μm. The red and blue lines indicate the measured spectrum at a bias current of 1.2 mA and the calculated spectrum with a refractive-index coupling coefficient of 1800 cm^{-1}, respectively.

After forming the electrodes and surface grating, the light-output properties were measured after cleaving the wafer in the passive waveguide. The measured bar consisted of 370-μm-long passive waveguide, 50-μm-long DFB laser, 500-μm-long passive waveguide, 50-μm-long DFB laser and 370-μm-long passive waveguide. The total bar length was 1340 μm. Therefore the passive waveguide section length from the cleaved facet to the DFB laser was 370 μm. Figure 5(a) shows the light–current (*L–I*) and voltage–current (*V–I*)characteristics of a waveguide-integrated LCI-membrane DFB laser with a cavity length, L_a, of 50 μm and a stripe width, W_s, of 0.8 μm under RT-CW conditions. A threshold current, I_{th}, of 230 μA and an external differential quantum efficiency, η_d, of 5% (from the front facet) were obtained. To the best of our knowledge, this value of the threshold current is a record low among the DFB lasers reported under RT-CW conditions. The threshold current density, J_{th}, was 575 A/cm^2 (115 A/cm^2/well), and the maximum output power from the front waveguide was 32 μW at an injection current of 1.3 mA. This low-threshold-current lasing was achieved thanks to the introduction of a strongly index-coupled grating structure with a short cavity structure for decreasing the active-region volume. We think the differential quantum efficiency can be improved to be approximately 40–50% by adopting a distributed-reflector (DR) structure and shortening the active region length to 20–30 μm together with increasing the index-coupling coefficient of the grating [26,27].The reduction of the optical loss in the passive waveguide region can be expected by using wire shaped waveguide without p-type doping [28]. Figure 5(b) shows the *L–I* characteristics for various operating temperatures under CW condition. Lasing operation was obtained up to 50°C.

Figure 6 shows the lasing spectrum of a waveguide-integrated LCI-membrane DFB laser for a device with a cavity length of 50 μm and a stripe width of 0.8 μm. In this figure, the red and blue lines respectively indicate the measured spectrum at a bias current of 1.2 mA and the calculated spectrum for an index-coupling coefficient, κ, of 1800 cm^{-1}.A lasing wavelength of 1534 nm and a submode suppression ratio (SMSR) of 28dB at this bias current. The stopband width was estimated to be 40 nm from the calculation even though it was not clearly observed in the measured spectrum. Resonant modes on the longer wavelength side of the stopband were very weak because this stopband width was wider than the gain spectrum of the multiple quantum wells.

4. Conclusion

We demonstrated low-threshold-current operation of a waveguide-integrated LCI-membrane DFB laser on a Si substrate with a short cavity and strong index-coupling coefficient under RT-CW conditions. To the best of our knowledge, a record-low threshold current of 230 μA

#232433 - $15.00 USD Received 13 Jan 2015; revised 6 Mar 2015; accepted 9 Mar 2015; published 17 Mar 2015

was obtained for a DFB laser, and an external differential quantum efficiency of 5% (front waveguide output) was obtained for a device with a cavity length of 50 μm and a stripe width of 0.8 μm. The maximum output power of 32 μW was obtained at an injection current of 1.3 mA. These results demonstrate that the membrane DFB laser is very attractive as an ultralow-power-consumption light source for on-chip optical interconnects.

Acknowledgments

The authors would like to thank Professors M. Asada, Y. Miyamoto, T. Mizumoto, and S. Akiba of the Tokyo Institute of Technology, Tokyo, Japan, for productive discussions and comments. This work was supported by JSPS KAKENHI grants, numbers 24246061, 25709026, 25420321, and 12J08092.

#232433 - $15.00 USD Received 13 Jan 2015; revised 6 Mar 2015; accepted 9 Mar 2015; published 17 Mar 2015